CrystEngComm

PAPER

View Article Online
View Journal | View Issue

Cite this: *CrystEngComm*, 2018, **20**, 6412

Photochromic and photomodulated luminescence properties of two metal–viologen complexes constructed by a tetracarboxylate-anchored bipyridinium-based ligand†

Lin-Ke Li,*[a] Hai-Yang Li,[a] Ting Li,[a] Li-Hong Quan,[a] Jing Xu,[a] Fu-An Li[b] and Shuang-Quan Zang *[a]

Received 9th August 2018,
Accepted 31st August 2018

DOI: 10.1039/c8ce01335g

rsc.li/crystengcomm

In this study, two metal–viologen complexes, formulated as $[Cd_{1.5}(H_2L)_{0.5}(Cl)_3(CH_3OH)]_n$ (**1**) and $[Eu_2(L)(NO_3)_4(HOCH_2CH_2OH)_2]_n$ (**2**), were constructed by a tetracarboxylate anchored bipyridinium-based ligand 1,1′-bis(3,5-dicarboxybenzyl)-4,4′-bipyridinium dichloride ($H_4L{\cdot}Cl_2$). Single-crystal X-ray analyses revealed that complex **1** featured a 2D-layered structure, while complex **2** showed a 1D "ladder-like" chain structure. The difference in the central metal ions, anions, solvent molecules, deprotonation degree of the tetracarboxylate ligand, coordination modes and conformations of the ligand have a great influence on the final structure. As expected, incorporation of the viologen moiety to the frameworks led to the predefined photochromism: when samples **1** and **2** were exposed to UV-visible light, a reversible color change from light yellow to blue/dark blue occurred. Moreover, complex **2** exhibited the characteristic emission of Eu(III) ion in the visible region, and it also displayed an interesting reversible tunable photo-induced luminescence switching behavior: under the irradiation of UV-vis light, the luminescence emission intensity of complex **2** gradually decreased and reached 15% of the starting value after 8 min. These results may not only help to further understand the structure–photoresponse relationships of viologen-based MOFs, but also help to guide the design and synthesis of luminescent materials with photo-modulated switching ability.

Introduction

In recent years, articles reporting metal–organic framework (MOFs) materials have exponentially increased because of their wide applications in gas storage, sensing, separation, drug delivery, catalysis, magnetism, *etc.*[1–8] Moreover, varieties of new application prospects have been developed, among which MOFs being investigated as chromic materials in response to external stimuli have attracted increasing interest. In well-defined structural MOFs, external stimuli such as light, heat, electricity, magnetism, mechanical force, solvent and water molecules induced chromic behaviors, which endowed these stimuli responsive MOF materials with enormous potential applications.[9–16] These chromic MOF materials could be used in optoelectronic and photochemical devices, smart windows, memory devices, photomagnetism, data storage, inkless and erasable printing, nondestructive luminescence readout field and molecular switches,[9–16] and so on.

With the aim of producing efficient functional chromic MOF materials, photoactive organic linkers with specific structures are a preferred selection. For this purpose, viologen-functionalized ligands have been widely used in the self-assembly process because the ligand itself can undergo electron-transfer (ET) to produce viologen radicals under external light, heat or electrical stimuli, resulting in a photo-, thermo- or electrochromic behavior, respectively.[17–20] Moreover, MOFs built using pre-modified viologen ligands could be used to design new photo-response materials, which may possess predetermined or improved physical/chemical properties because of the highly ordered arrangement of functional ligands and metal ions.

In recent years, our group has been using various aromatic carboxylate-anchored bipyridinium/viologen-based ligands to react with different metal ions to construct functional photo-responsive MOF materials.[21] The incorporation of redox-active viologen groups can endow the as-synthesized MOF

[a] *College of Chemistry and Molecular Engineering, Zhengzhou University, Zhengzhou, 450001, P. R. China. E-mail: lilinke@zzu.edu.cn, zangsqzg@zzu.edu.cn*
[b] *College of Chemistry and Environment Engineering, Pingdingshan University, Pingdingshan, 467000, P. R. China*

† Electronic supplementary information (ESI) available. CCDC Crystallographic data in CIF format, tables of selected bond distances and angles, TGA, experimental and calculated powder XRD patterns and IR spectra. CCDC reference numbers 1859387 and 1859388 for complexes **1** and **2**. For ESI and crystallographic data in CIF or other electronic format see DOI: 10.1039/c8ce01335g

materials with charge transport properties as well as response to external stimuli. Moreover, the abundant oxygen atoms in the carboxylate groups and the pyridine nitrogen atoms are in favor of viologen-functionalized ligands' bonding with a variety of metal ions (which involve nearly the entire periodic table) to form the desired and fascinating structures.

Moreover, in most cases, lanthanide ions are excellent luminescent centers due to the high color purity and long lifetimes of their excited states.[22] In addition, Ln-MOFs usually present excellent luminescent characteristics when strong absorbing chromophores that can stimulate fluorescence emission from lanthanide ions are incorporated as adjacent antennas or sensitizers.[23] Aromatic carboxylate-anchored bipyridinium/viologen-based ligands have a large electron conjugated system, and may act as excellent "antennas" to induce the enhancement of fluorescence intensity upon coordination with lanthanide ions. Photo-response properties of the functional viologen-based ligand in combination with the excellent luminescence of Ln(III) complexes may result in MOF materials with multi-functional properties.

Therefore, under the guidance of these considerations, using a tetracarboxylate anchored bipyridinium-based ligand 1,1′-bis(3,5-dicarboxybenzyl)-4,4′-bipyridinium dichloride ($H_4L\cdot Cl_2$) to react with transition and lanthanide metal ions, two metal–viologen MOFs, formulated as $[Cd_{1.5}(H_2L)_{0.5}(Cl)_3(CH_3OH)]_n$ (**1**) and $[Eu_2(L)(NO_3)_4(HOCH_2CH_2OH)_2]_n$ (**2**), were prepared. Furthermore, the reversible photochromism of complexes **1** and **2** as well as the solid-state luminescence and photo-modulated luminescence switching properties of complex **2** were investigated. Additionally, powder X-ray diffraction (PXRD) analyses, infrared spectroscopy (IR) analyses, elemental analyses, thermogravimetric analyses (TGA) and electron-spin resonance spectroscopy (ESR) analyses of these MOFs have been performed.

Experimental

Materials and methods

Ligand 1,1′-bis(3,5-dicarboxybenzyl)-4,4′-bipyridinium dichloride ($H_4L\cdot Cl_2$) (Scheme 1) was synthesized according to a literature procedure with some modifications.[24] All other commercially available reagents were used without further purification. Elemental analyses for C, H and N were performed using a Perkin-Elmer 240 elemental analyzer. IR spectra were recorded with KBr pellets in the range of 4000–400 cm^{-1} on a Bruker VECTOR 22 spectrometer. Thermogravimetric analyses were performed using a TA Q50 thermal analyzer from room temperature to 800 °C with a heating rate of 10 °C min^{-1} under nitrogen flow. Powder X-ray diffraction (PXRD) patterns for complexes **1** and **2** were recorded on a Rigaku D/Max-3B diffractometer (Cu Kα, λ = 1.5418 Å) in the 2θ range of 5–50°. Crushed single crystalline powder samples were prepared by crushing the crystals and scanning from 5° to 50° with a step of 0.1° s^{-1}. Solid UV-visible spectrum was obtained in the 200–800 nm range on a JASCOUVIDEC-660 spectrophotometer. Electron-spin resonance (ESR) signals were recorded on a Brucker A300 spectrometer at room temperature.

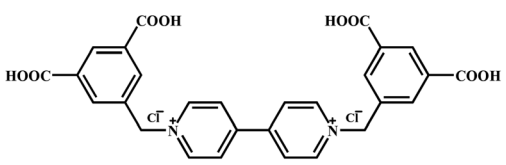

Scheme 1 The ligand 1,1′-bis(3,5-dicarboxybenzyl)-4,4′-bipyridinium dichloride ($H_4L\cdot Cl_2$).

Preparation

Synthesis of $[Cd_{1.5}(H_2L)_{0.5}(Cl)_3(CH_3OH)]_n$ (1). $Cd(Cl)_2\cdot 2.5H_2O$ (21 mg, 0.045 mmol) and $H_4L\cdot Cl_2$ (9 mg, 0.015 mmol) were dissolved in the mixed solvent of methanol/acetonitrile (3 mL/1 mL) in a 25 mL Teflon-lined stainless steel vessel and heated at 85 °C for 48 hours. The mixture was then cooled to room temperature at a rate of 6 °C h^{-1}. The colorless block crystals of **1** were obtained in a yield of 85% based on Cd. Anal. calcd. for $C_{30}H_{28}N_2O_{10}Cl_6Cd_3$ (1126.50) (%): C, 31.99; H, 2.50; N, 2.49%; found (%): C, 32.53; H, 2.31; N, 2.59%. IR/cm^{-1} (KBr): 3419 (s), 1685 (vs), 1639 (m), 1564 (vs), 1444 (m), 1365 (s), 1338 (m), 1290 (w), 1199 (s), 1108 (w), 1006 (s), 923 (w), 840 (w), 755 (m), 719 (w), 671 (w), 578 (w).

Synthesis of $[Eu(L)_{0.5}(NO_3)_2(HOCH_2CH_2OH)]_n$ (2). A mixture of $Eu(NO_3)_3\cdot 6H_2O$ (27 mg, 0.06 mmol) and $H_4L\cdot Cl_2$ (18 mg, 0.03 mmol) was added to the mixed solvent of acetonitrile/glycol (2 mL/0.5 mL) in a 25 mL Teflon-lined stainless steel vessel. The mixture was heated at 90 °C for 72 hours and then slowly cooled to the room temperature at a rate of 3 °C h^{-1}. Pale yellow block crystals were obtained. Yield: 80% based on Eu. Anal. calcd. for $C_{32}H_{30}N_6O_{24}Eu_2$ (1186.53) (%): C, 32.39; H, 2.55; N, 7.08%; found (%): C, 32.68; H, 2.59; N, 7.00%. IR/cm^{-1} (KBr): 3415 (m), 1637 (m), 1560 (m), 1455 (s), 1384 (vs), 1332 (s), 1302 (m), 1214 (w), 1157 (m), 1069 (m), 917 (w), 890 (w), 865 (w), 813 (w), 731 (m), 688 (w), 565 (w).

X-ray crystallography. Single crystal X-ray analyses were conducted on a Bruker SMART APEX CCD diffractometer using graphite-monochromatized Mo Kα radiation (λ = 0.71073 Å) at room temperature using the ω-scan technique. Lorentz polarization and absorption corrections were applied. The structures were solved by direct methods with SHELXS-97 (ref. 25) and refined by full-matrix least-squares using the SHELXL-97 (ref. 26) program. All non-hydrogen atoms were refined anisotropically. The hydrogen atoms of the ligands were included in the structure factor calculation at idealized positions using a riding model and refined isotropically. Hydrogen atoms of the solvent water molecules were located from difference Fourier maps, and then restrained at fixed positions and refined isotropically. Analytical expressions of neutral atom scattering factors were employed, and anomalous dispersion corrections were incorporated. Crystallographic data and selected bond distances and angles for complexes **1** and **2** are listed in Tables S1 and S2 (ESI†).

Crystallographic data were deposited with the Cambridge Crystallographic Data Center (CCDC) as supplementary publication numbers CCDC 1859387 and 1859388 for **1** and **2**, respectively.

Results and discussion

Crystal structure of $[Cd_{1.5}(H_2L)_{0.5}(Cl)_3(CH_3OH)]_n$ (1)

Complex **1** crystallizes in a triclinic space group $P\bar{1}$ and features a 2D-layered structure. The asymmetric unit of **1** consists of one and a half independent Cd(II) cations (the occupancy is 1 for Cd1 and 0.5 for Cd2), one half of an H_2L ligand, three coordinated Cl^- ions and one coordinated CH_3OH molecule.

As shown in Fig. 1, in the crystal structure, both Cd(II) centers are six-coordinated, but in different coordination environments. Each Cd1 ion is coordinated by two carboxylate oxygen atoms (O1 and O4#1) from two H_2L ligands in different coordination modes (one is in monodentate coordination mode and the other is in bridging mode) and four Cl^- ions (Cl1, Cl2, Cl3 and Cl1#2), among which Cl1, Cl3 and Cl1#2 take part in the coordination in bridging mode, while Cl2 is in monodentate mode, forming a slightly distorted octahedral geometry (Fig. 1). Cl1, Cl2, Cl1#2 and O4#1 compose the equatorial plane (the mean derivation from the ideal $CdCl_3O$ plane is 0.0333 Å), while Cl2 and O1 exist on the axial positions; the axial angle is 171.37(8)°. The resulting CdO_2Cl_4 octahedron exhibits Cd1–O bond lengths of 2.300(3) and 2.442(3) Å, and Cd1–Cl bond distances in the range of 2.5071(12)–2.7271(11) Å (Table S2†). For Cd2, the CdO_4Cl_2 core shows a nearly perfect octahedral geometry. The coordination is provided by two oxygen atoms (O3#1 and O3#5) from two different H_2L ligands in bidentate bridging mode, two oxygen atoms (O5 and O5#4) from coordinated CH_3OH molecules and two bridging Cl^- ions (Cl3 and Cl3#4), as shown in Fig. 1. The four oxygen atoms compose the equatorial plane (the mean derivation from the ideal CdO_4 plane is 0.000 Å), and the Cd–O bond distances 2.264(3) and 2.385(3) Å. The O–Cd2–O bond angles are nearly 90° or 180°. The other two Cl^- ions exist on the axial positions, and the axial angle is 180°. The Cd2–Cl bond length is 2.6385(12) Å and the Cl–Cd2–Cl bond angle is 180° (Table S2†). These values are all comparable to the other reported values of Cd(II)–viologen complexes.[27]

As for the ligand $H_4L{\cdot}Cl_2$, Wriedt *et al.* had used the ligand $H_4bdcbpyBr_2{\cdot}2H_2O$ (1,1′-bis(3,5-dicarboxybenzyl)-4,4′-bipyridinium dibromide dihydrate solvate) to construct two isostructural MOFs $\{[M\text{-}(bdcbpy)(OH_2)_4]{\cdot}4H_2O\}_n$ (M = Mn and Ni), in which the ligand $H_4bdcbpyBr_2$, was fully deprotonated in the framework, yielding the anionic ligand $bdcbpy^{2-}$ to coordinate with the metal ions and counterbalance the M^{2+} metal clusters in MOFs.[24] In this study, complex **1** possesses a partially deprotonated $H_4L{\cdot}Cl_2$ ligand, in which only two protons (H^+) of the carboxylate groups are removed, yielding the neutral ligand H_2L bearing no charge. The H_2L ligand presents *trans*-conformation. Furthermore, one H_2L ligand bridges with six Cd(II) ions in two types of coordination modes: μ_2-η^1:η^1 mode and μ_1-η^1:η^0 mode. The O atoms connect with Cd2 only in the μ_2-η^1:η^1 mode. Cd1 and Cd2 atoms are linked by one bridging carboxylate group from one H_2L ligand and one bridging Cl^- ion, forming a Cd_3 unit (Cd1Cd2Cd1). The Cd_3 units are repeated along the chain, and di-Cl-bridges connect the repeating Cd_3 units. These Cd_3 units are located nearly on a straight line. The adjacent Cd···Cd distances in one line are 4.0294(4) Å and 4.2054(4) Å. In addition, these two types of intervals are alternatively arranged along the line, with the adjacent Cd···Cd···Cd angles of 173.45(1)° and 180.00(0)°. All the Cd(II) ions are in a strict plane, forming the skeleton of the 2-D layer along the *bc* plane (Fig. 2).

In the H_2L ligand, the two pyridinium rings of the same ligand are also in a nearly ideal plane (mean deviation from the ideal plane is 0.0076 Å), and the two aromatic carboxylate moieties have the same included angles with the central pyridinium rings (111.26°) but towards different directions. The 3,5-dicarboxybenzyl units are significantly twisted from the neighboring pyridinium rings with dihedral angles of 75.63°; hence, the ligand H_2L presents *trans*-conformation.

The adjacent layers are connected by C–H···Cl hydrogen bond interactions (H bond distance is 3.594 Å and the bond angle is 145.28°). Moreover, the adjacent aromatic carboxylate rings in one layer are parallel to each other along the *a* direction, and the nearest centroid to centroid distance is 3.785 Å.

Depending on the hydrogen bonding interactions and intermolecular forces, the 2D layered structure is extended into the 3D solid-state packed structure (Fig. 3).

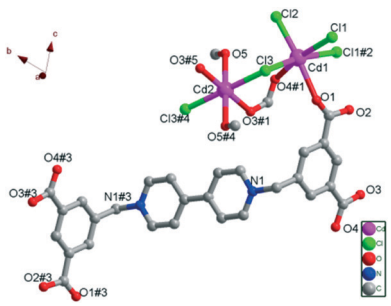

Fig. 1 Perspective view of the coordination environment of Cd(II) ions in **1** (hydrogen atoms are omitted for clarity). Symmetry codes: #1: $-x + 2, -y, -z + 1$; #2: $-x + 1, -y, -z + 2$; #3: $-x + 2, -y + 1, -z$; #4: $-x + 1, -y + 1, -z + 1$; #5: $x - 1, y + 1, z$.

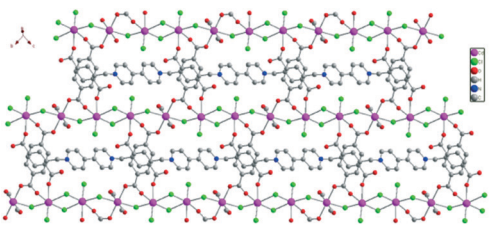

Fig. 2 The 2D layered structure of complex **1**. All hydrogen atoms are omitted for clarity.

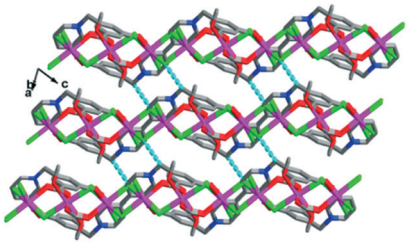

Fig. 3 3D solid-state packed structure of complex **1** with the existence of C–H···Cl hydrogen bonds between the close packed layers.

Crystal structure of complex $[Eu(L)_{0.5}(NO_3)_2(HOCH_2CH_2OH)]_n$ (2)

Single-crystal X-ray diffraction analysis revealed that complex **2** crystallized in the triclinic space group $P\bar{1}$ and featured a 1D "ladder-like" chain structure. As shown in Fig. 4, the asymmetric unit of **2** has one Eu(III) ion, one half of a L^{2-} ligand, two coordinated nitrate ions and one coordinated glycol molecule. Eu1 is ten-coordinated to four oxygen atoms of two nitrate ions in η^2-chelation mode, four oxygen atoms of two carboxylate groups in η^2-chelation mode, and two oxygen atoms from one glycol molecule also in η^2-chelation mode. The Eu–O bond lengths are in the range of 2.431(7) to 2.710(8) Å, and the bond angles around the Eu(III) center are in the range of 93.99(9)° to 129.20(9)° (Table S2†), which are comparable to those of other reported Eu(III)–oxygen complexes.

The coordination geometry of the completely deprotonated ligand L^{2-} was greatly different from that of a recently reported 3D Eu(III) framework constructed by the same ligand, *viz.*, $[Eu_2(OH)_2(H_2O)_2L]Cl_2{\cdot}8H_2O$,[28] in which the tetracarboxylate ligand adopts a U-shaped conformation with each carboxylate in the μ-η^2:η^1 coordination mode while chelating a metal ion and bridging another metal ion through a μ-O atom. However, in this case, the ligand L^{2-} still adopts the Z-shaped *trans*-conformation similar to that in complex **1** and participates in coordinating in μ_4-η^2:η^2:η^2:η^2 mode to connect the adjacent four Eu(III) ions to form a 1D chain along the *b* direction (Fig. 5). The four Eu(III) ions connected by the same L^{2-} ligand form a parallelogram, with Eu···Eu lengths of 9.909 × 17.891 Å^2. All the pyridinium rings and aromatic carboxylate rings in the same line are parallel to each other along the *b* direction. The two pyridinium rings of the same ligand are in a nearly ideal plane (mean deviation from the ideal plane is 0.0118 Å), and the two aromatic carboxylate moieties have the same included angles with the central pyridinium rings (108.7(8)°) but towards different directions, forming the Z shaped conformation (Fig. 5). The 3,5-dicarboxybenzyl units are significantly twisted from the neighboring pyridinium rings with dihedral angles of 73.46°, which is close to that of the former two complexes. The adjacent chains along the *c* direction are interlaced and parallel to each other, with the nearest centroid to centroid distance between the aromatic carboxylates being 3.940 Å, indicating the existence of weak face-to-face aromatic π···π interactions. These weak π···π interactions closely pack the 1D chains to form 2D layers (Fig. 5).

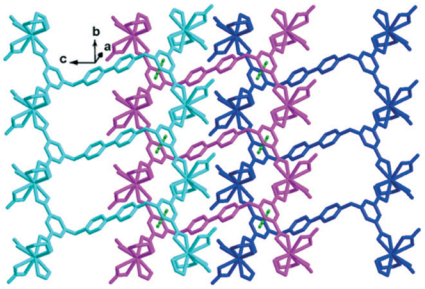

Fig. 5 The 2D layered structure of complex **2** formed by weak π···π interactions (green dotted line). All hydrogen atoms are omitted for clarity.

Furthermore, the weak π···π interactions and weak intermolecular forces tightly connect the 2D layers to form the 3D solid-state structure (Fig. 6).

Thermostability, PXRD patterns and IR

Powder X-ray diffraction (PXRD), thermogravimetric analysis (TGA) and IR (infrared) spectroscopy patterns before and after light irradiation were obtained to confirm the stability of these frameworks (ESI†).

TGA measurements of complexes **1** and **2** were performed from room temperature to 800 °C under nitrogen atmosphere to evaluate the thermal stability of the two complexes (Fig. S1†). For complex **1**, upon heating, the first experimental weight loss of 5.46% from 220 to 255 °C roughly corresponds to the release of two methanol molecules (calculated 5.69%). Upon further heating, after a plateau, the weight loss corresponds to the decomposition of organic moieties in the range

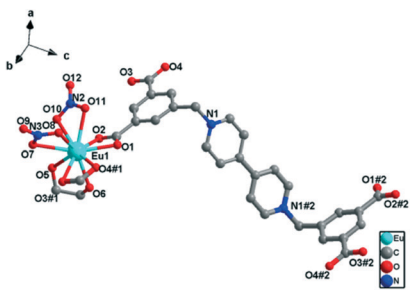

Fig. 4 Perspective view of the coordination environment of the Eu(III) ion in **2** (hydrogen atoms are omitted for clarity). Symmetry codes: #1: *x*, *y* + 1, *z*, #2: −*x*, 1 − *y*, 3 − *z*.

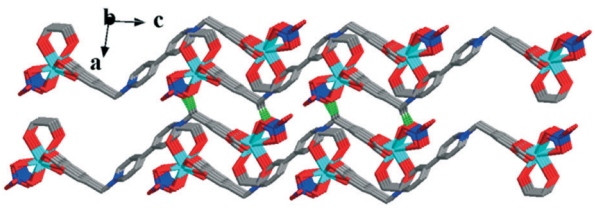

Fig. 6 The solid-state structure of complex **2** formed by hydrogen bonds and weak π···π interactions.

of 315 to 700 °C. In case of complex **2**, the framework remained stable up to 225 °C and then, the two-step weight loss occurred from 225 to 396 °C, corresponding to the release of two coordinated glycol molecules and four coordinated nitrate anions. The subsequent weight loss is ascribed to the decomposition of the organic moiety.

The phase purity of the two complexes has been investigated by X-ray diffraction. As shown in Fig. S2 (ESI†), the peak positions of theoretical and experimental as well as the PXRD patterns before and after the irradiation agree well with each other, indicating the high purity and homogeneity of these complexes; also, this result showed that the structures are maintained during photochromism.

IR (Fig. S3, ESI†) spectra of complexes **1** and **2** before and after the irradiation as well as after thermal bleaching also coincided well, indicating that the framework was maintained before and after the treatment. The results also indicated that the photochromism was not caused by isomerization or photolysis. The photochromic processes of complexes **1** and **2** could be probably ascribed to the electron-transfer and the photo-induced generation of viologen radicals.

Photochromic properties

Complexes **1** and **2** were photosensitive, giving a visible color change within a few minutes upon the exposure to sunlight or the xenon lamp (300 W) in air at room temperature. Complex **1** turned from pale yellow to blue, and the coloration achieved complete saturation after irradiation for 15 minutes (Fig. 7a). Photo-induced blue crystals (**1**-L) regained the pale yellow color after being kept in the dark for about two days under ambient conditions or in 20 min by heating at 120 °C in air. The color of complex **2** changed from pale yellow to dark blue, and the coloration achieved complete saturation after irradiation for 10 minutes (Fig. 7b). In addition, the photo-induced product (**2**-L) could regain the light yellow color when maintained in the dark for one day under ambient conditions or in about 15 min by heating at 120 °C in air. Such reversible color transformations could be repeated for several continuous cycles without a noticeable color loss, indicating good reversible properties of the two complexes.

UV-vis reflectance spectra were recorded before and after illumination (Fig. 7). From the figure, we can observe that the photoproducts exhibited two characteristic bands at 403 nm and 612 nm for complex **1** and 404 nm and 625 nm for complex **2**, which increase gradually with the duration of irradiation. These absorption peaks should be related to π–π* and *n*–π* transitions of the conjugated ligand L^{2-}.

After irradiation, ESR spectra displayed strong and sharp signals at g = 2.0018 and 2.0019 for **1** and **2**, respectively (Fig. 8), which are close to that of a free electron (2.0023) and can be assigned to radicals.[20,21,29] Furthermore, the intensities of the signals of the complexes drastically increased with the irradiation time, confirming the formation of radicals. These features resemble those of photogenerated viologen radicals.[20,21,29] Thus, the photochromic behaviors of complexes **1** and **2** could be ascribed to the photoinduced electron transfer and the generation of free viologen radicals.

The solid-state UV-vis reflectance spectrum of the ligand $H_4L{\cdot}Cl_2$ was also recorded for comparison (Fig. S4†). It only shows one peak in the ultraviolet region, and the ligand itself has no photochromic property. Thus, the photochromic behaviors of the complexes are ascribed to the influence of the crystal structure.

In an attempt to gain an in-depth understanding of the influence of the structure on the photochromic behaviors, the detailed structural analyses of the complexes were performed carefully. As mentioned in previous reports, for viologen-based MOFs, several factors such as the distance between the donor and the acceptor, the orientation between the electron donor and the acceptor, the packing type, hydrogen bonding interactions, C–H···π interactions,[17–21,24,29] as well as halide anions···acceptor interaction[30] may have a great influence on the final photochromic behaviors. In case of the two complexes, these are still the main factors to be considered. For complex **1**, the shortest distance between the carboxylate oxygen atom and the N^+ of the pyridinium ring is 3.387 Å, the shortest distance between the Cl atom and the N^+ of the pyridinium ring is 3.421 Å and the δ angles between the donor-N^+ line and the normal of the pyridinium plane are about 22.34° and 67.64°, respectively (Fig. S5†). Furthermore, the existence of weak π–π stacking interactions between the aromatic rings in neighboring bipyridinium ligands and the hydrogen bonding interactions also are favorable for electron transfer between the donor and the acceptor. For complex **2**, as the central metal ion Eu(III) is a lanthanide metal ion, it instinctively exhibits high oxophilicity (hard acid hard base interaction)[31,32] and usually coordinates strongly to the

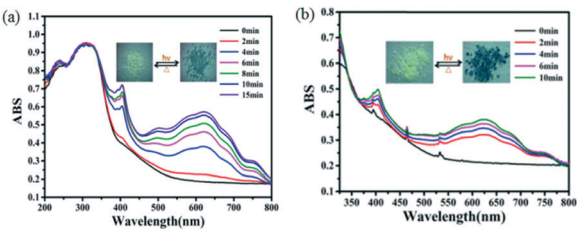

Fig. 7 UV-vis spectra and photographs showing the photochromic behaviors of complexes **1** (a) and **2** (b), the inset is the colour change of the complexes **1** and **2** before and after irradiation.

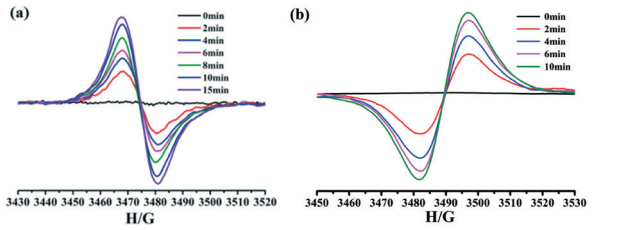

Fig. 8 The ESR spectra for complexes **1** (a) and **2** (b) before and after the irradiation in the solid state at room temperature.

oxygen donor. Thus, the abundant O atoms in the coordination environment, originating from carboxylate groups and the coordinated nitrate anions, provided much more donor···acceptor electron transfer pathways. Furthermore, the shortest O···N distance is 3.456 Å, while the other O···N distances are 3.664, 3.708 and 3.779 Å, respectively (Fig. S5†). The δ angles between the donor-N^+ line and the normal of the pyridinium plane are about 67.64°, 22.34°, 24.72° and 25.24°. These distances and angles are all favorable for electron transfer. At the same time, weak offset π···π interactions between the aromatic carboxylates also contributed to the photochromic behavior of complex **2**.

Photoluminescence properties

Lanthanide MOFs have usually shown good luminescence properties in terms of their high color purity. Hence, we also investigated the ligand-assisted photoluminescence properties of solid-state samples of the Eu(III) complex at room temperature. Moreover, for metal–viologen complexes, photoluminescence modulation property has also been observed and it has attracted considerable attention in recently reported chromic MOF materials.[17,20,33]

The solid-state luminescent property of ligand $H_4L{\cdot}Cl_2$ was characterized by recording a UV-vis reflectance spectrum (Fig. S4†). It is observed that in the spectral region from 230 to 400 nm, ligand $H_4L{\cdot}Cl_2$ exhibits one intense broad excitation band centered at about 300 nm, with a rapidly decreasing tail in the visible light region.

The solid-state photoluminescence behavior of complex **2** before and after irradiation was also investigated. Excitation of the as-synthesized solid of complex **2** at room temperature resulted in peaks at 361, 375, 395, 414, 464 and 532 nm, which were ascribed to the electron transitions of $^7F_0 \rightarrow {}^5D_4$, $^7F_0 \rightarrow {}^5L_7$, $^7F_0 \rightarrow {}^5L_6$, $^7F_0 \rightarrow {}^5D_3$, $^7F_0 \rightarrow {}^5D_2$ and $^7F_1 \rightarrow {}^5D_1$, respectively (Fig. 9a).

Under the excitation of 395 nm at room temperature, the typical red emission of the Eu(III) ion in the visible region was detected for complex **2** (Fig. 9b), and the five sharp peaks appearing at 578, 586, 616, 646 and 690 nm correspond to the characteristic f–f transitions of $^5D_0 \rightarrow {}^7F_J$ (J = 0–4) of Eu(III) ions. Similar to the other Eu(III) complexes, the electric dipole $^5D_0 \rightarrow {}^7F_2$ transition is the strongest among all the transitions, and it is responsible for the bright red luminescence of the complex. Moreover, since the fluorescence intensity ratio of $^5D_0 \rightarrow {}^7F_2$ to $^5D_0 \rightarrow {}^7F_1$ is sensitive to the structural change in the vicinity of Eu(III) ions, the intensity ratio (*ca.* 7) of $I(^5D_0 \rightarrow {}^7F_2)/I(^5D_0 \rightarrow {}^7F_1)$ indicated the low symmetry of the Eu(III) site in complex **2**.[34] This is consistent with the crystal structure analysis.

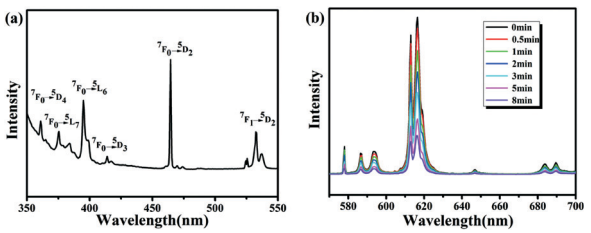

Fig. 9 (a) Solid-state excitation spectrum of complex **2** at room temperature. (b) The luminescence emission spectral changes (λ_{ex} = 395 nm) of complex **2** with the time of irradiation.

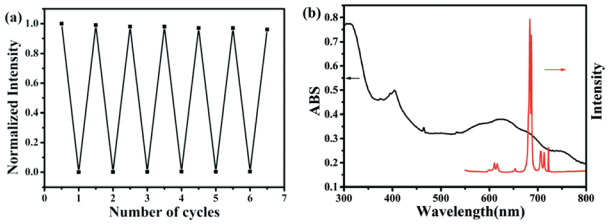

Fig. 10 (a) The repeated switching of luminescence emission of complex **2** between the initial and colored states based on photochromic modulation. (b) The luminescence emission spectra of complex **2** and the ligand in the solid-state at room temperature.

It has been reported that viologen radicals are typical luminescence quenchers.[35] Under the irradiation of UV light, the luminescence emission intensity (395 nm) of complex **2** exhibited a gradual decrease with time and reaches 15% of the starting value after 8 min (as shown in Fig. 9b). The photoswitching process can be repeated several times without a noticeable loss in luminescence intensity (Fig. 10a). As for the reason of luminescent switching, we can surmise a conclusion from Fig. 10b: there exists a spectral overlap between the emission band of the initial sample and the broad UV-vis absorption band of the colored sample, which can result in the energy transfer from the excited luminescent center to the L^{2-} free radical. Thus, the luminescence switching behaviors of complex **2** were induced. This photomodulated luminescence switching behavior combined with photochromism is an interesting property, which may result in more and broad application prospects for this type of metal–viologen complexes in the photoactivity field.

Conclusions

In summary, utilizing an aromatic polycarboxylate-anchored bipyridinium-based ligand to react with different metal ions, two metal–viologen complexes with different structures have been successfully synthesized. The central metal ions, deprotonation degree of polycarboxylate groups, and the coordination geometry of viologen-based ligands have a great impact on the final structure of MOFs, and further result in their distinct photochromic behaviors. Moreover, when coordinated with the luminescent lanthanide Eu(III) metal ion, the final complex exhibits characteristic emission of Eu(III) ion in the visible region, and the viologen-based ligand could act as an effective "antenna" to induce the enhancement of fluorescence intensity. The existence of the viologen moiety induced the photomodulated luminescence change in the Eu(III)–viologen MOF. The structural analyses of these complexes revealed that the electron transfer between the carboxylate-O

donor and the pyridinium-N acceptor is the dominating factor for photochromic behaviors. Moreover, the abundant O atoms in the tetracarboxylate anchored bipyridinium-based ligand provide much more electron transfer pathways, which increase the possibility for the effective electron transfer to happen, thus resulting in the occurrence of the photochromic behaviour.

Systematic investigations on this type of MOF materials are still underway to search for more chromic materials. The results obtained in this paper can not only help to understand the structure–photosensitivity relationships of viologen-based MOF systems, but also guide the design and synthesis of more luminescent materials with photomodulated luminescence switching properties.

Conflicts of interest

There are no conflicts to declare.

Acknowledgements

This study was supported by the National Natural Science Foundation of China (No. 21371153 and 21801227), Key Scientific Research Project Plan in Colleges and Universities of Henan Province (16A150045) and Scientific and technological project in Henan Province (162102410070) and Zhengzhou University student innovation and entrepreneurship training program (2018cxcy006).

Notes and references

1 L. Ungur, S. Y. Lin, J. Tang and L. F. Chibotaru, *Chem. Soc. Rev.*, 2014, **43**, 6894–6905.

2 A. Bianchi, E. Delgado-Pinar, E. García-España, C. Giorgi and F. Pina, *Coord. Chem. Rev.*, 2014, **260**, 156–215; M. Irie, T. Fukaminato, K. Matsuda and S. Kobatake, *Chem. Rev.*, 2014, **114**, 12174–12277.

3 J. Liu, P. K. Thallapally, B. P. McGrail, D. R. Brown and J. Liu, *Chem. Soc. Rev.*, 2012, **41**, 2308–2322; N. C. Burtch, H. Jasuja and K. S. Walton, *Chem. Rev.*, 2014, **114**, 10575–10612; M. P. Suh, H. J. Park, T. K. Prasad and D.-W. Lim, *Chem. Rev.*, 2012, **112**, 782–835; Q. Gao, J. Xu, D. P. Cao, Z. Chang and X.-H. Bu, *Angew. Chem., Int. Ed.*, 2016, **55**, 15027–15030.

4 H. Wang, J. Xu, D.-S. Zhang, Q. Chen, R.-M. Wen, Z. Chang and X.-H. Bu, *Angew. Chem., Int. Ed.*, 2015, **54**, 5966–5970; Z. Xie, L. Ma, K. E. DeKrafft, A. Jin and W. Lin, *J. Am. Chem. Soc.*, 2010, **132**, 922–923; L. Lu, J. Wu, J. Wang, J.-Q. Liu, B.-H. Li, A. Singh, A. Kumar and S. R. Batten, *CrystEngComm*, 2017, **19**, 7057–7067.

5 J.-R. Li, J. Sculley and H.-C. Zhou, *Chem. Rev.*, 2012, **112**, 869–932; B. Van de Voorde, B. Bueken, J. Denayer and D. De Vos, *Chem. Soc. Rev.*, 2014, **43**, 5766–5788; Q. Y. Yang, D. H. Liu, C. L. Zhong and J.-R. Li, *Chem. Rev.*, 2013, **113**, 8261–8323.

6 D. Cunha, M. Ben Yahia, S. Hall, S. R. Miller, H. Chevreau, E. Elkaïm, G. Maurin, P. Horcajada and C. Serre, *Chem. Mater.*, 2013, **25**, 2767–2776; P. Horcajada, R. Gref, T. Baati, P. K. Allan, G. Maurin, P. Couvreur, G. Férey, R. E. Morris and C. Serre, *Chem. Rev.*, 2012, **112**, 1232–1268.

7 A. H. Chughtai, N. Ahmad, H. A. Younus, A. Laypkovc and F. Verpoort, *Chem. Soc. Rev.*, 2015, **44**, 6804–6849; M. Yoon, R. Srirambalaji and K. Kim, *Chem. Rev.*, 2012, **112**, 1196–1231; C. J. Doonan and C. J. Sumby, *CrystEngComm*, 2017, **19**, 4044–4048.

8 P. Dechambenoit and J. R. Long, *Chem. Soc. Rev.*, 2011, **40**, 3249–3265; J.-P. Zhao, J. Xu, S.-D. Han, Q.-L. Wang and X.-H. Bu, *Adv. Mater.*, 2017, **29**, 1606966; X.-M. Meng, L.-S. Cui, X.-P. Wang, X.-Y. Zhang, X. Zhang and S.-Y. Bi, *CrystEngComm*, 2017, **19**, 6630–6643.

9 J. T. Sampanthar, K. G. Neoh, S. W. Ng, E. T. Kang and K. L. Tan, *Adv. Mater.*, 2000, **12**, 1536–1539; G. Mehlana and S. A. Bourne, *CrystEngComm*, 2017, **19**, 4238–4259.

10 V. Stavila, A. A. Talin and M. D. Allendorf, *Chem. Soc. Rev.*, 2014, **43**, 5994–6010.

11 S. Kawata and Y. Kawata, *Chem. Rev.*, 2000, **100**, 1777–1788.

12 M. D. Ward, J. R. White and A. J. Bard, *J. Am. Chem. Soc.*, 1983, **105**, 27–31.

13 L.-Z. Cai, Q.-S. Chen, C.-J. Zhang, P.-X. Li, M.-S. Wang and G.-C. Guo, *J. Am. Chem. Soc.*, 2015, **137**, 10882–10885; J.-H. Li, S.-D. Han, J. Pan, Z.-Z. Xue, G.-M. Wang, Z.-H. Wang and Z.-Z. Bao, *CrystEngComm*, 2017, **19**, 1160–1164.

14 B. Garai, A. Mallick and R. Banerjee, *Chem. Sci.*, 2016, **7**, 2195–2200; R. Zou, J. Zhang, S. Z. Hu, F. Hu, H. Y. Zhang and Z. F. Fu, *CrystEngComm*, 2017, **19**, 6259–6262.

15 X.-D. Yang, L. Sun, C. Chen, Y.-J. Zhang and J. Zhang, *Dalton Trans.*, 2017, **46**, 4366–4372; X.-D. Yang, C. Chen, Y.-J. Zhang, L.-X. Cai, B. Tan and J. Zhang, *Dalton Trans.*, 2016, **45**, 4522–4527; J. Kärnbratt, M. Hammarson, S. Li, H. L. Anderson, B. Albinsson and J. Andréasson, *Angew. Chem., Int. Ed.*, 2010, **49**, 1854–1857; J.-K. Sun, L.-X. Cai, Y.-J. Chen, Z.-H. Li and J. Zhang, *Chem. Commun.*, 2011, **47**, 6870–6872.

16 P.-X. Li, M.-S. Wang, M.-J. Zhang, C.-S. Lin, L.-Z. Cai, S.-P. Guo and G.-C. Guo, *Angew. Chem., Int. Ed.*, 2014, **53**, 11529–11531; F. Luo, C. B. Fan, M. B. Luo, X. L. Wu, Y. Zhu, S. Z. Pu, W.-Y. Xu and G.-C. Guo, *Angew. Chem., Int. Ed.*, 2014, **53**, 9298–9301; W.-B. Li, Q.-X. Yao, L. Sun, X.-D. Yang, R.-Y. Guo and J. Zhang, *CrystEngComm*, 2017, **19**, 722–726.

17 G. Xu, G.-C. Guo, M.-S. Wang, Z.-J. Zhang, W.-T. Chen and J.-S. Huang, *Angew. Chem., Int. Ed.*, 2007, **46**, 3249–3251; X.-S. Xing, Z.-W. Chen, L.-Z. Cai, C. Sun, L.-R. Cai, M.-S. Wang and G.-C. Guo, *RSC Adv.*, 2016, **6**, 24190–24194; M.-S. Wang, C. Yang, G.-E. Wang, G. Xu, X.-Y. Lv, Z.-N. Xu, R.-G. Lin, L.-Z. Cai and G.-C. Guo, *Angew. Chem., Int. Ed.*, 2012, **51**, 3432–3435.

18 C. H. Zhang, L. B. Sun, Y. Yan, H. Z. Shi, B. L. Wang, Z. Q. Liang and J. Y. Li, *J. Mater. Chem. C*, 2017, **5**, 8999–9004; H. Chen, M. Li, G. Zheng, Y. Wang, Y. Song, C. Han, Z. Fu, S. Liao and J. Dai, *RSC Adv.*, 2014, **4**, 42983–42990; X.-H. Jin, C.-X. Ren, J.-K. Sun, X.-J. Zhou, L.-X. Cai and J. Zhang, *Chem. Commun.*, 2012, **48**, 10422–10424; X.-H. Jin, J.-K. Sun, L.-X. Cai and J. Zhang, *Chem. Commun.*, 2011, **47**, 2667–2669.

19 J.-K. Sun, P. Wang, C. Chen, X.-J. Zhou, L.-M. Wu, Y.-F. Zhang and J. Zhang, *Dalton Trans.*, 2012, **41**, 13441–13446;

J.-K. Sun, P. Wang, Q.-X. Yao, Y.-J. Chen, Z.-H. Li, Y.-F. Zhang, L.-M. Wu and J. Zhang, *J. Mater. Chem.*, 2012, **22**, 12212–12219; X.-H. Jin, J.-K. Sun, X.-M. Xu, Z.-H. Li and J. Zhang, *Chem. Commun.*, 2010, **46**, 4695–4697.

20 H.-X. Zhang, Q.-X. Yao, X.-H. Jin, Z.-F. Ju and J. Zhang, *CrystEngComm*, 2009, **11**, 1807–1810; Q.-X. Yao, Z.-F. Ju, X.-H. Jin and J. Zhang, *Inorg. Chem.*, 2009, **48**, 1266–1268; Q.-X. Yao, L. Pan, X.-H. Jin, J. Li, Z.-F. Ju and J. Zhang, *Chem. – Eur. J.*, 2009, **15**, 11890–11897; C. H. Zhang, L. B. Sun, C. Q. Zhang, S. Wan, Z. Q. Liang and J. Y. Li, *Inorg. Chem. Front.*, 2016, **3**, 814–820; C. Y. Tao, J. B. Wu, Y. Yan, C. Shi and J. Y. Li, *Inorg. Chem. Front.*, 2016, **3**, 541–546.

21 H.-Y. Li, Y.-L. Wei, X.-Y. Dong, S.-Q. Zang and T. C. W. Mak, *Chem. Mater.*, 2015, **27**, 1327–1331; H.-Y. Li, H. Xu, S.-Q. Zang and T. C. W. Mak, *Chem. Commun.*, 2016, **52**, 525–528; H.-Y. Li, J. Xu, L.-K. Li, X.-S. Du, F.-A. Li, H. Xu and S.-Q. Zang, *Cryst. Growth Des.*, 2017, **17**, 6311–6319.

22 J.-C. G. Bünzli and C. Piguet, *Chem. Soc. Rev.*, 2005, **34**, 1048–1077.

23 Y. J. Cui, Y. F. Yue, G. D. Qian and B. L. Chen, *Chem. Rev.*, 2012, **112**, 1126–1162.

24 D. Aulakh, J. R. Varghese and M. Wriedt, *Inorg. Chem.*, 2015, **54**, 1756–1764; T. Gong, X. Yang, J.-J. Fang, Q. Sui, F.-G. Xi and E.-Q. Gao, *ACS Appl. Mater. Interfaces*, 2017, **9**, 5503–5512; D. Aulakh, A. P. Nicoletta, J. R. Varghese and M. Wriedt, *CrystEngComm*, 2016, **18**, 2189–2202.

25 G. M. Sheldrick, *Acta Crystallogr., Sect. A: Found. Crystallogr.*, 1990, **46**, 457; G. M. Sheldrick, *SHELXS-97, Program for solution of crystal structures*, University of Göttingen, Germany, 1997.

26 G. M. Sheldrick, *SHELXL-97, Program for refinement of crystal structures*, University of Göttingen, Germany, 1997.

27 J.-J. Liu, Y.-F. Guan, M.-J. Lin, C.-C. Huang and W.-X. Dai, *Cryst. Growth Des.*, 2016, **16**, 2836–2842.

28 T. Gong, P. Li, Q. Sui, J. Q. Chen, J. H. Xu and E.-Q. Gao, *J. Mater. Chem. A*, 2018, **6**, 9236–9244.

29 E. M. Kosower and J. L. Cotter, *J. Am. Chem. Soc.*, 1964, **86**, 5524–5527; M. Kaneko, J. Motoyoshi and A. Yamada, *Nature*, 1980, **285**, 468–470; P. M. S. Monk, *The Viologens: Physicochemical Properties, Synthesis and Applications of the Salts of 4,4'-Bipyridine*, John Wiley & Sons, New York, 1998; P.-X. Li, M.-S. Wang, L.-Z. Cai, G.-E. Wang and G.-C. Guo, *J. Mater. Chem. C*, 2015, **3**, 253–256; T. Gong, X. Yang, Q. Sui, Y. Qi, F.-G. Xi and E.-Q. Gao, *Inorg. Chem.*, 2016, **55**, 96–103.

30 X.-Y. Lv, M.-S. Wang, C. Yang, G.-E. Wang, S.-H. Wang, R.-G. Lin and G.-C. Guo, *Inorg. Chem.*, 2012, **51**, 4015–4019; N. Leblanc, W. H. Bi, N. Mercier, P. Auban-Senzier and C. Pasquier, *Inorg. Chem.*, 2010, **49**, 5824–5833; F. Wan, L.-X. Qiu, L.-L. Zhou, Y.-Q. Sun and Y. You, *Dalton Trans.*, 2015, **44**, 18320–18323.

31 M. Watanabe, T. Nankawa, T. Yamada, T. Kimura, K. Namiki, M. Murata, H. Nishihara and S. Tachimori, *Inorg. Chem.*, 2003, **42**, 6977–6979.

32 V. Patroniak, P. N. W. Baxter, J.-M. Lehn, Z. Hnatejko and M. Kubicki, *Eur. J. Inorg. Chem.*, 2004, 2379–2384.

33 X.-H. Jin, J.-K. Sun, X.-M. Xu, Z.-H. Li and J. Zhang, *Chem. Commun.*, 2010, **46**, 4695–4697; J. B. Wu, Y. Yan, B. K. Liu, X. L. Wang, J. Y. Li and J. H. Yu, *Chem. Commun.*, 2013, **49**, 4995–4997; G. Xu, G.-C. Guo, J.-S. Guo, S.-P. Guo, X.-M. Jiang, C. Yang, M.-S. Wang and Z.-J. Zhang, *Dalton Trans.*, 2010, **39**, 8688–8692.

34 S. Sivakumar, M. L. P. Reddy, A. H. Cowley and R. R. Butorac, *Inorg. Chem.*, 2011, **50**, 4882–4891; M. Fernandes, V. de Zea Bermudez, R. A. SáFerreira, L. D. Carlos, A. Charas, J. Morgado, M. M. Silva and M. Smith, *J. Mater. Chem.*, 2007, **19**, 3892–3901; J. Xia, B. Zhao, H. S. Wang, W. Shi, Y. Ma, H. B. Song, P. Cheng, D. Z. Liao and S. P. Yan, *Inorg. Chem.*, 2007, **46**, 3450–3458; S. Biju, D. B. Ambili Raj, M. L. P. Reddy and B. M. Kariuki, *Inorg. Chem.*, 2006, **45**, 10651–10660.

35 A. Beneduci, S. Cospito, M. L. Deda and G. Chidichimo, *Adv. Funct. Mater.*, 2015, **25**, 1240–1247.